Continuous Carbon Fiber Polymer-Matrix Composites and Their Joints, Studied by Electrical Measurements

D. D. L. CHUNG

Composite Materials Research Laboratory
State University of New York at Buffalo
Buffalo, N.Y. 14260-4400

Continuous carbon fiber polymer-matrix composites and their joints, as studied by DC electrical measurements, are reviewed. The resistance gives information on the microstructure and allows the self-sensing of strain, damage and temperature. In the case of composites with dissimilar fibers in adjacent laminae, the Seebeck effect allows temperature sensing, using the interface between laminae as a thermocouple junction. The resistance in the through-thickness direction can be apparently negative, due to entropy-driven electron backflow. The longitudinal resistance allows sensing of the glass transition and melting of the thermoplastic polymer matrix. The quality of composite-composite joints obtained by adhesion or fastening, and of composite-concrete joints obtained by adhesion, is revealed by resistance measurements.

INTRODUCTION

Polymer-matrix composites containing continuous carbon fibers are important structural materials due to their high tensile strength, high tensile modulus and low density. They are used for lightweight structures such as satellites, aircraft, automobiles, bicycles, ships, submarines, sporting goods, wheel chairs, armor and rotating machinery (such as turbine blades and helicoptor rotors). Due to the recent emphasis on repair of civil infrastructural systems, composites are beginning to be used for the repair of concrete structures and for bridges, even though they are much more expensive than concrete. As the price of carbon fibers has been dropping steadily during the last two decades, the spectrum of applications has been widening tremendously.

The continuous carbon fibers used are primarily either based on polyacrylonitrile (PAN) or mesophase pitch. Mesophase-pitch-based carbon fibers, if heat treated to high temperatures exceeding 2500°C, can be graphitized and attain very high values of the tensile modulus and thermal conductivity (in-plane), in addition to improved oxidation resistance. The high thermal conductivity is attractive for thermal management, which is particularly important for electronics (i.e., heat sinks, etc.). However, the graphitized fibers tend to be relatively low in strength, due to the ease of shear between the graphite layers, and they are very expensive. On the other hand, PAN-based fibers cannot be graphitized, though they compete well with mesophase-pitch-based fibers which have not been graphitized, in that both materials exhibit reasonably high values of both strength and modulus and are not very expensive. These fibers are the most widely used among carbon fibers. The fabrication of both pitch-based and PAN-based carbon fibers involves stabilization (infusibilization) and then carbonization (conversion from hydrocarbon molecules to a carbon network). Graphitization optionally follows carbonization.

Due to the importance of carbon fiber polymer-matrix composites for structural applications, much investigation has been made on the mechanical behavior of these materials. Much less work has been done to study the electrical behavior (1–8). On the other hand, due to the fact that carbon fibers are much more conducting than the polymer matrix, the electrical behavior gives much information on the microstructure, such as the degree of fiber alignment, the number of fiber-fiber contacts, the amount of delamination and the extent of fiber breakage. Such information is not only useful for scientific understanding of the properties of the composite, but is also valuable for the purpose of rendering the composite the ability to sense its strain, damage and temperature in real time via electrical measurement. In other words, the strain, damage and temperature affect the electrical behavior, such as the electrical resistance, which thus serves to indicate strain, damage and temperature. In this way, the composite is self-sensing, i.e., intrinsically smart, without the need for attached or embedded sensors (such as optical fibers, acoustic sensors and piezoelectric sensors), which raise the cost, reduce the durability and, in the case of embedded sensors, weaken the structure.

Smart structures are structures that have the ability to sense certain stimuli and be able to response to the stimuli in an appropriate fashion, somewhat like a human being. Sensing is the most fundamental aspect of a smart structure. A structural composite which is itself a sensor is multifunctional. The sensing of strain is needed for structural vibration control, which is important for rotating machinery, satellites, aircraft and sporting goods. The sensing of damage is needed for structural health monitoring, which is valuable for all important structures. The sensing of temperature is useful for thermal control and thermal hazard mitigation. The sensing of temperature-induced phase transformations, such as the glass transition and melting of the polymer matrix, is useful for polymer matrix characterization.

This paper addresses the electrical behavior of continuous carbon fiber polymer-matrix composites in static and dynamic conditions. The static condition refers to the situation without stimuli. The dynamic condition refers to the situation in which the strain, damage or temperature varies and the effect of the variation is monitored in real time.

This paper also addresses the electrical behavior of a composite which is in contact with another piece of the same type of composite, or with another material (such as concrete). A composite-composite contact is relevant to joining, whether by adhesion (such as autohesion in the case of a thermoplastic) or pressure (as in fastening). Joining is an important process in the manufacture of a composite structure. A composite-concrete contact attained by adhesion is relevant to the use of composites to repair concrete structures.

As epoxy is the dominant matrix material for carbon fiber polymer-matrix composites, this paper emphasizes epoxy-matrix composites. However, composites with thermoplastic matrices are also addressed.

This paper does not address the practical implementation of the electrical methods in composite structures, due to the infancy of the field. However, the content of this paper provides the basis for practical implementation.

BASIC BEHAVIOR

Carbon fibers are electrically conducting, while the polymer matrix is electrically insulating [except for the rare situation in which the polymer is an electrically conducting one (9)]. The continuous fibers in a composite laminate are in the form of layers called laminae. Each lamina comprises many bundles (called tows) of fibers in a polymer matrix. Each tow consists of thousands of fibers. There may or may not be twist in a tow. Each fiber has a diameter typically ranging from 7 to 12 μm. The tows within a lamina are typically oriented in the same direction, but tows in different laminae may or may not be in the same direction. A laminate with tows in all the laminae oriented in the same direction is said to unidirectional. A laminate with tows in adjacent laminae oriented at an angle of 90° is said to be crossply.

Within a lamina with tows in the same direction, the electrical conductivity is highest in the fiber direction. In the transverse direction in the plane of the lamina, the conductivity is not zero, even though the polymer matrix is insulating. This is because there are contacts between fibers of adjacent tows (10). In other words, a fraction of the fibers of one tow touch a fraction of the fiber of an adjacent tow here and there along the length of the fibers. These contacts result from the fact that fibers are not perfectly straight or parallel (even though the lamina is said to be unidirectional), and that the flow of the polymer matrix (or resin) during composite fabrication can cause a fiber to be not completely covered by the polymer or resin (even though, prior to composite fabrication, each fiber may be completely covered by the polymer or resin, as in the case of a prepreg, i.e., a fiber sheet impregnated with the polymer or resin). Fiber waviness is known as marcelling. Thus, the transverse conductivity gives information on the number of fiber-fiber contacts in the plane of the lamina.

For similar reasons, the contacts between fibers of adjacent laminae cause the conductivity in the through-thickness direction (direction perpendicular to the plane of the laminate) to be non-zero. Thus, the through-thickness conductivity gives information on the number of fiber-fiber contacts between adjacent laminae.

Matrix cracking between the tows of a lamina decreases the number of fiber-fiber contacts in the plane of the lamina, thus decreasing the transverse conductivity. Similarly, matrix cracking between adjacent laminae [as in delamination (11)] decreases the number of fiber-fiber contacts between adjacent laminae, thus decreasing the through-thickness conductivity. This means that the transverse and through-thickness conductivities can indicate damage in the form of matrix cracking.

Fiber damage (as distinct from fiber fracture) decreases the conductivity of a fiber, thereby decreasing the longitudinal conductivity (conductivity in the fiber direction). However, due to the brittleness of carbon fibers, the decrease in conductivity due to fiber damage prior to fiber fracture is rather small (12).

Fiber fracture causes a much larger decrease in the longitudinal conductivity of a lamina than fiber damage. If there is only one fiber, a broken fiber results in an open circuit, i.e., zero conductivity. However, a lamina has a large number of fibers and adjacent fibers can make contact here and there. Therefore, the portions of a broken fiber still contribute to the longitudinal conductivity of the lamina. As a result, the decrease in conductivity due to fiber fracture is less than what it would be if a broken fiber did not contribute to the conductivity. Nevertheless, the effect of fiber fracture on the longitudinal conductivity is significant, so that the longitudinal conductivity can indicate damage in the form of fiber fracture (13).

The through-thickness volume resistance of a laminate is the sum of the volume resistance of each of

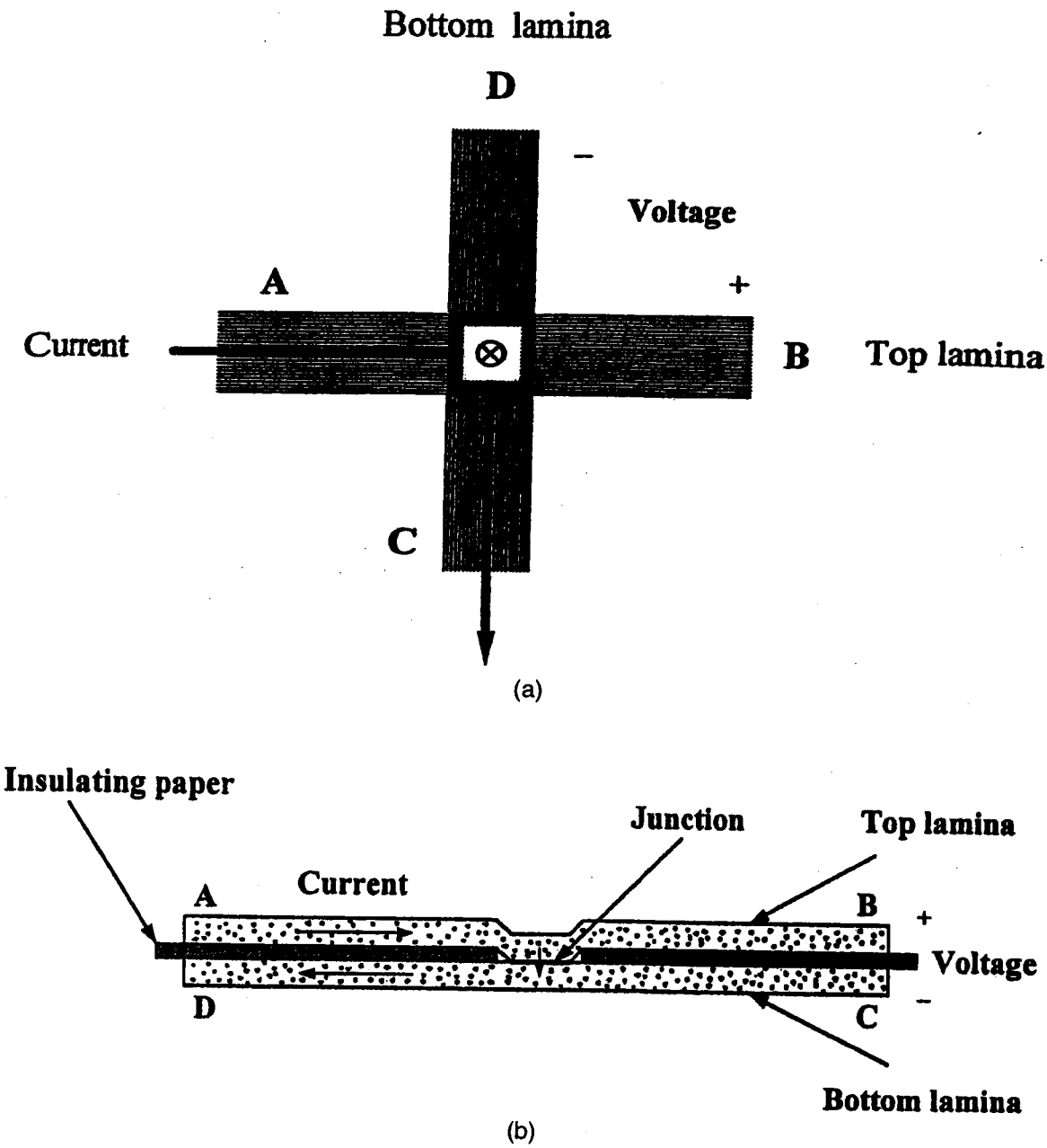

Fig. 1. Specimen configuration for measurement of the contact electrical resistivity between laminae. (a) Crossply laminae. (b) Unidirectional laminae.

the laminae in the through-thickness direction and the contact resistance of each of the interfaces between adjacent laminae (i.e., the interlaminar interface). For example, a laminate with eight laminae has eight volume resistances and seven contact resistances, all in the through-thickness direction. Thus, to study the interlaminar interface, it is better to measure the contact resistance between two laminae rather than the through-thickness volume resistance of the entire laminate.

Measurement of the contact resistance between laminae can be made by allowing two laminae (strips) to contact at a junction and using the two ends of each strip for making four electrical contacts (14). An end of the top strip and an end of the bottom strip serve as contacts for passing current. The other end of the top strip and the other end of the bottom strip serve as contacts for voltage measurement. The fibers in the two strips can be in the same direction or in different directions. This method is a form of the four-probe method of electrical resistance. The configuration is illustrated in *Fig. 1* for crossply and unidirectional laminates. To make sure that the volume resistance within a lamina in the through-thickness direction does not contribute to the measured resistance, the fibers at each end of a lamina strip should

electrically shorted together by using silver paint or other conducting media. The measured resistance is the contact resistance of the junction. This resistance, multiplied by the area of the junction, gives the contact resistivity, which is independent of the area of the junction and just depends on the nature of the interlaminar interface. The unit of the contact resistivity is $\Omega.m^2$, whereas that of the volume resistivity is $\Omega.m$.

The structure of the interlaminar interface tends to be more prone to change than the structure within a lamina. For example, damage in the form of delamination is much more common than damage in the form of fiber fracture. Moreover, the structure of the interlaminar interface is affected by the interlaminar stress (whether thermal stress or curing stress), which is particularly significant when the laminae are not unidirectional (as the anisotropy within each lamina enhances the interlaminar stress). The structure of the interlaminar interface also depends on the extent of consolidation of the laminae during composite fabrication. The contact resistance provides a sensitive probe of the structure of the interlaminar interface.

The measurement of the volume resistivity in the through-thickness direction can be conducted by using the four-probe method, in which each of the two current contacts is in the form of a conductor loop (made by silver paint, for example) on each of the two outer surfaces of the laminate in the plane of the laminate and each of the two voltage contacts is in the form of a conductor dot within the loop (11). An alternate method is to have four of the laminae in the laminate be extra long so as to extend out for the purpose of serving as electrical leads (15). The two outer leads are for current contacts, the two inner leads are for voltage contacts. The use of a thin metal wire inserted at an end into the interlaminar space during composite fabrication in order to serve as an electrical contact is not recommended, because the quality of the electrical contact between the metal wire and carbon fibers is hard to control and the wire is intrusive to the composite. The alternate method is less convenient than the method involving loops and dots, but it approaches more closely the ideal four-probe method.

In order to attain zero conductivity in the through-thickness direction of a laminate, it is necessary to use an insulating layer between two adjacent laminae (16). The insulating layer can be a piece of writing paper. Tissue paper is ineffective in preventing contacts between fibers of adjacent laminae, due to its porosity. The attainment of zero conductivity in the through-thickness direction allows the laminate to serve as a capacitor. This means that the structural composite stores energy by serving as a capacitor.

STRAIN EFFECTS

Self-monitoring of strain (reversible) has been achieved in carbon fiber epoxy-matrix composites without the use of embedded or attached sensor (17–21), as the electrical resistance of the composite in the through-thickness or longitudinal direction changes reversibly with longitudinal strain (gauge factor up to 40) due to change in the degree of fiber alignment. Tension in the fiber direction of the composite increases the degree of fiber alignment, thereby decreasing the chance for fibers of adjacent laminae to touch one another. As a consequence, the through-thickness resistance increases while the longitudinal resistance decreases.

Figure 2 (22) shows the change in longitudinal resistance during cyclic longitudinal tension in the elastic regime for a unidirectional continuous carbon fiber epoxy-matrix composite with eight fiber layers (laminae). The stress amplitude is equal to 14% of the breaking stress. The strain returns to zero at the end of each cycle. Because of the small strains involved, the fractional resistance change $\Delta R/R_0$ is essentially equal to the fractional change in resistivity. The longitudinal $\Delta R/R_0$ decreases upon loading and increases upon unloading in every cycle, such that R irreversibly decreases slightly after the first cycle (i.e., $\Delta R/R_0$ does not return to 0 at the end of the first cycle). At higher stress amplitudes, the effect is similar, except that both the reversible and irreversible parts of $\Delta R/R_0$ are larger.

Figure 3 (22) shows the change in the through-thickness resistance during cyclic longitudinal tension in the elastic regime for the same composite. The stress amplitude is equal to 14% of the breaking stress. The through-thickness $\Delta R/R_0$ increases upon loading and decreases upon unloading in every cycle, such that R irreversibly decreases slightly after the first cycle (i.e., $\Delta R/R_0$ does not return to 0 at the end of the first cycle). Upon increasing the stress amplitude, the effect is similar, except that the reversible part of $\Delta R/R_0$ is larger.

The strain sensitivity (gauge factor) is defined as the reversible part of $\Delta R/R_0$ divided by the longitudinal strain amplitude. It is negative (from −18 to −12) for the longitudinal $\Delta R/R_0$ and positive (from 17 to 24) for the through-thickness $\Delta R/R_0$. The magnitudes are comparable for the longitudinal and through-thickness strain sensitivities. As a result, whether the longitudinal R or the through-thickness R is preferred for strain sensing just depends on the convenience of electrical contact application for the geometry of the particular smart structure.

Figure 4 (22) shows the compressive stress, strain and longitudinal $\Delta R/R_0$ obtained simultaneously during cyclic compression at stress amplitudes equal to 14% of the breaking stress for a similar composite having 24 rather than 8 fiber layers. The longitudinal $\Delta R/R_0$ increases upon compressive loading and decreases upon unloading in every cycle, such that resistance R irreversibly increases very slightly after the first cycle. The magnitude of the gauge factor is lower in compression (−1.2) than in tension (from −18 to −12).

A dimensional change without any resistivity change would have caused longitudinal R to increase during

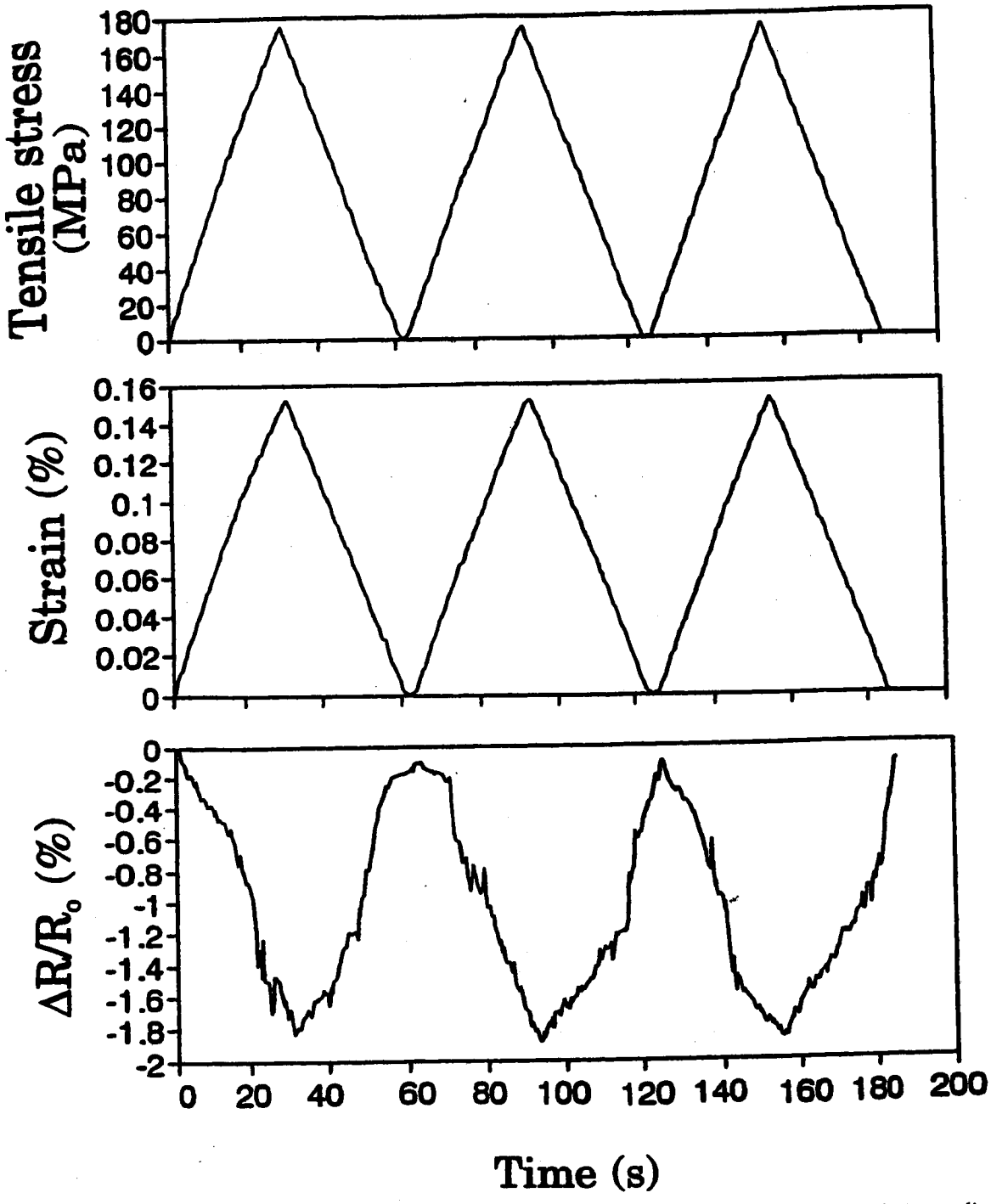

Fig. 2. Longitudinal stress and strain and fractional resistance increase ($\Delta R/R_0$) obtained simultaneously during cyclic tension at a stress amplitude equal to 14% of the breaking stress for continuous fiber epoxy-matrix composite.

tensile loading and decrease during compressive loading. In contrast, the longitudinal R decreases upon tensile loading and increases upon compressive loading. In particular, the magnitude of $\Delta R/R_0$ under tension is 7–11 times that of $\Delta R/R_0$ calculated by assuming that $\Delta R/R_0$ is only due to dimensional change and not due to any resistivity change. Hence the contribution of $\Delta R/R_0$ from the dimensional change is negligible compared to that from the resistivity change.

The irreversible behavior, though small compared to the reversible behavior, is such that R (longitudinal or through-thickness) under tension is irreversibly decreased after the first cycle. This behavior is attributed

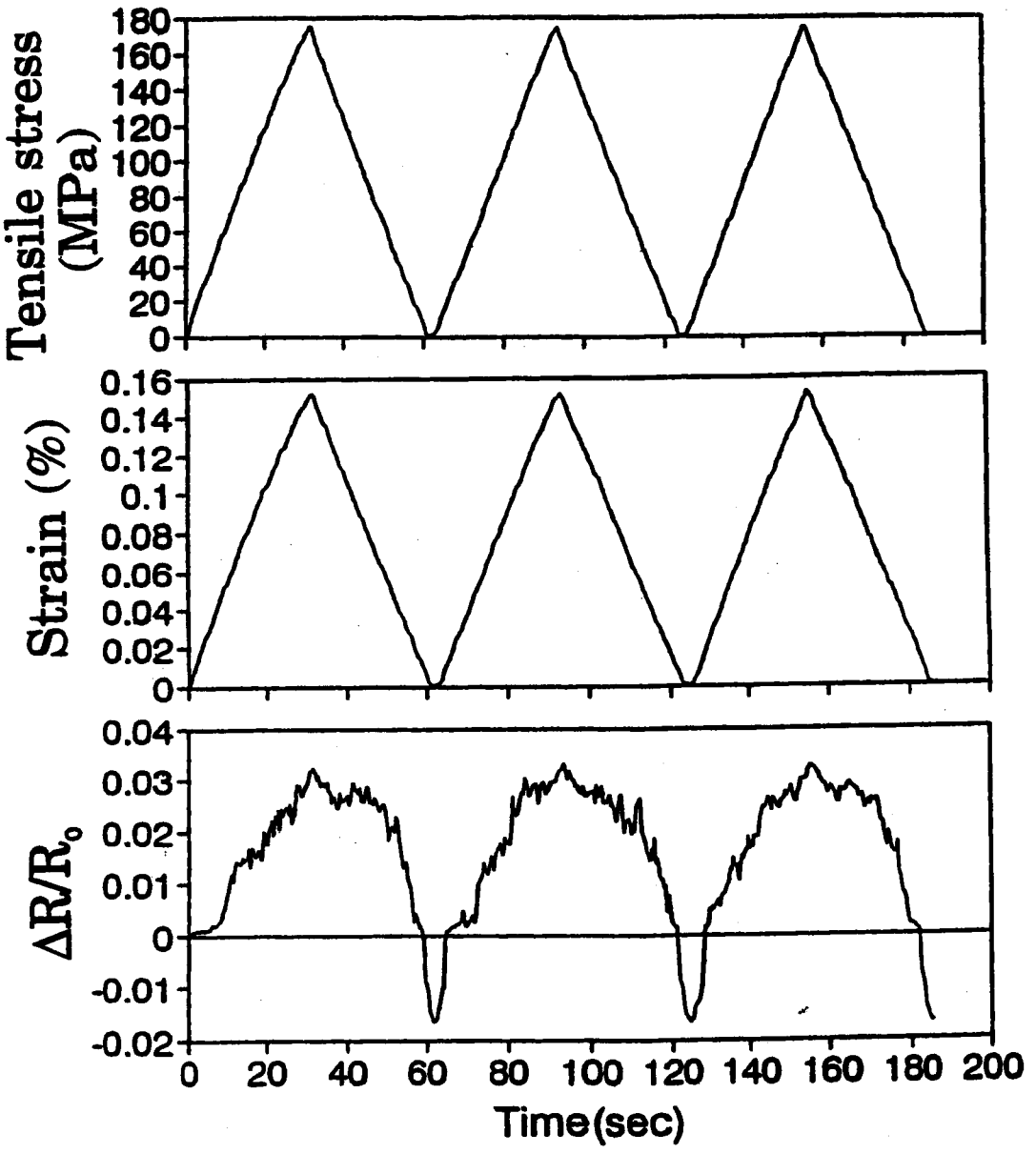

Fig. 3. Longitudinal stress and strain and the through-thickness $\Delta R/R_0$ obtained simultaneously during cyclic tension at a stress amplitude equal to 14% of the breaking stress for continuous fiber epoxy-matrix composite.

to the irreversible disturbance to the fiber arrangement at the end of the first cycle, such that the fiber arrangement becomes less neat or less ordered. A less neat fiber arrangement means more chance for the adjacent fiber layers to touch one another.

DAMAGE EFFECTS

Self-monitoring of damage (whether due to stress or temperature, under static or dynamic conditions) has been achieved in continuous carbon fiber polymer-matrix composites, as the electrical resistance of the composite changes with damage (11, 15, 17, 22–34). Minor damage in the form of slight matrix damage and disturbance to the fiber arrangement is indicated by the longitudinal and through-thickness resistance decreasing irreversibly due to increase in the number of contacts between fibers, as shown after one loading cycle in *Fig. 2* and *3*. Major damage in the form of delamination is indicated by the through-thickness resistance increasing irreversibly due to decrease in the number of contacts between fibers of different laminae. Major damage in the form of fiber breakage is indicated by the longitudinal resistance increasing irreversibly. During mechanical fatigue, delamination was observed to begin at 30% of the fatigue life, whereas fiber breakage was observed to begin at 50% of the

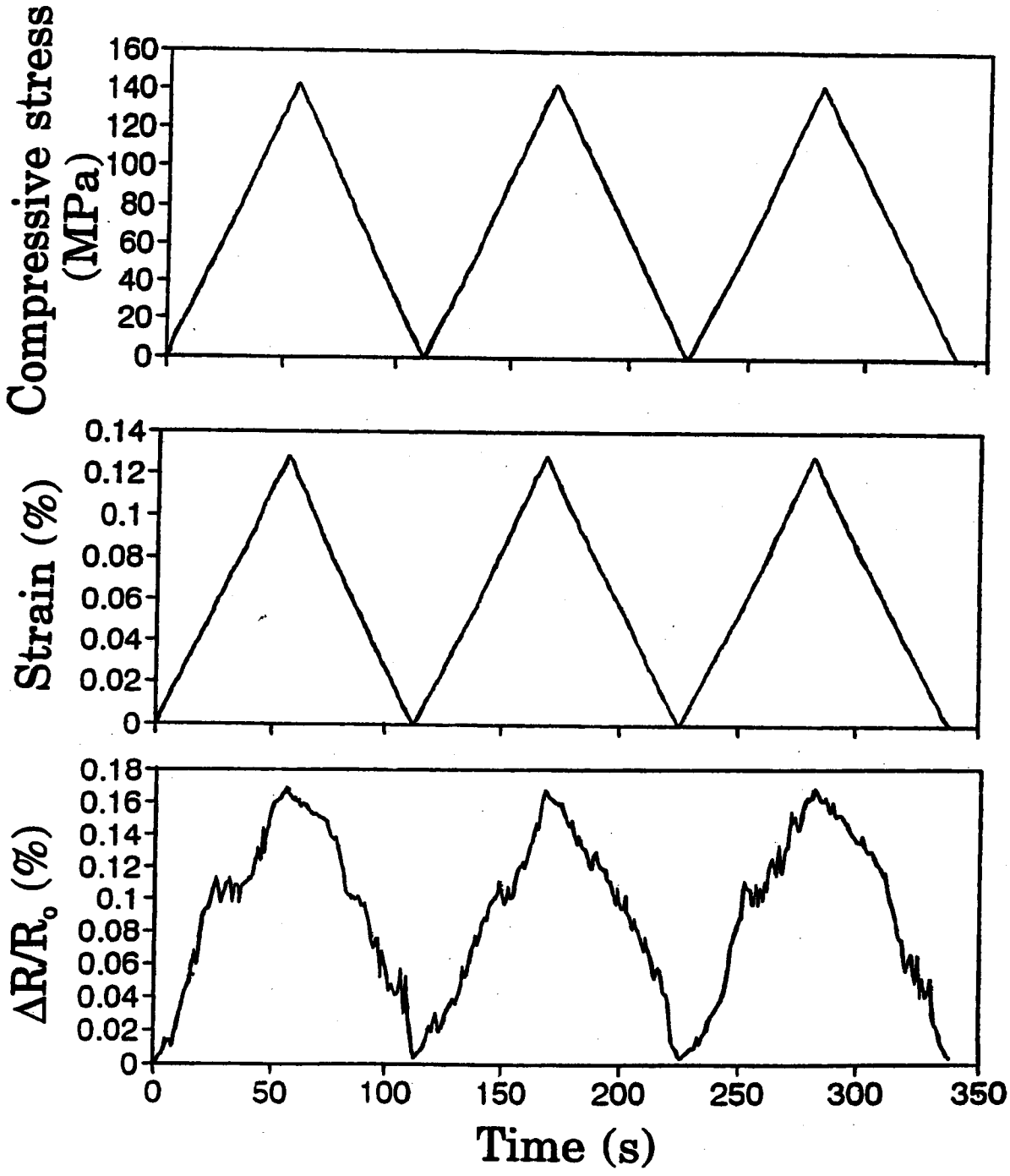

Fig. 4. Longitudinal stress, strain and $\Delta R/R_0$ obtained simultaneously during cyclic compression (longitudinal) at a stress amplitude equal to 14% of the breaking stress for continuous fiber epoxy-matrix composite.

fatigue life. *Figure 5* (22) shows an irreversible resistance increase occurring at about 50% of the fatigue life during tension-tension fatigue testing of a unidirectional continuous carbon fiber epoxy-matrix composite. The resistance and stress are in the fiber direction. The reversible changes in resistance are due to strain, which causes the resistance to decrease reversibly in each cycle, as in *Fig. 2*.

TEMPERATURE EFFECTS (THERMISTOR EFFECT)

Continuous carbon fiber epoxy-matrix composite provide temperature sensing by serving as thermistors (35) and thermocouples (36).

The thermistor function stems from the reversible decrease of the contact electrical resistivity at

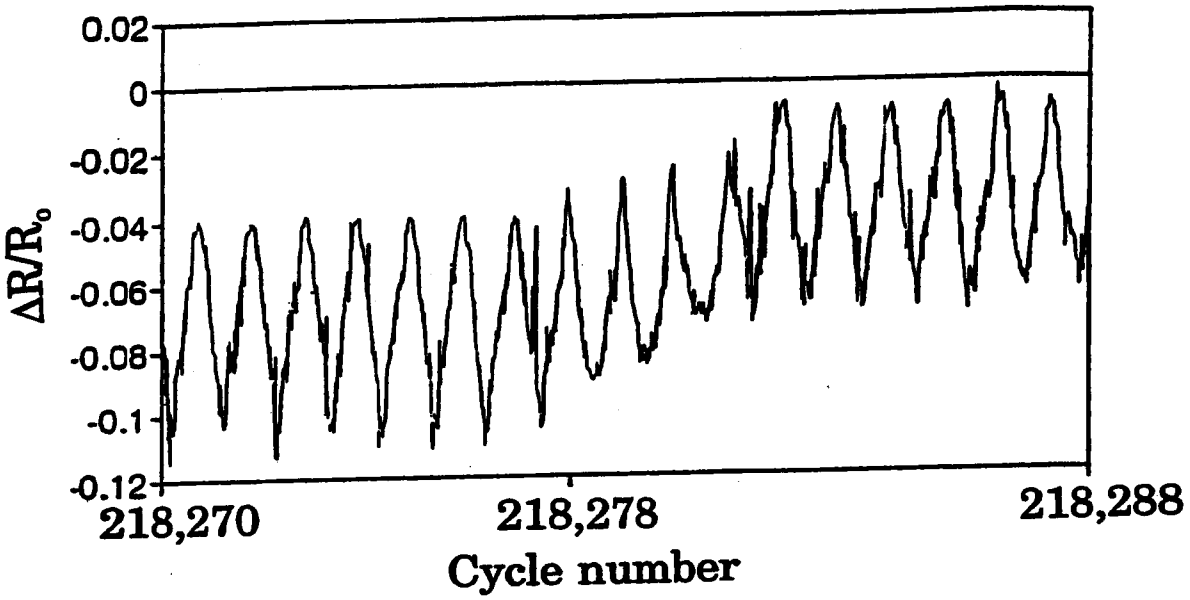

Fig. 5. Variation of longitudinal $\Delta R/R_0$ with cycle number during tension-tension fatigue testing for a carbon fiber epoxy-matrix composite. Each cycle of reversible decrease in resistance is due to strain. The irreversible increase in resistance at around cycle no. 218,281 is due to damage in the form of fiber breakage.

interface between fiber layers (laminae) on temperature. *Figure 6* shows the variation of the contact resistivity ρ_c with temperature during reheating and subsequent cooling, both at 0.15°C/min, for carbon fiber epoxy-matrix composites cured at 0 and 0.33 MPa. The corresponding Arrhenius plots of log contact conductivity (inverse of contact resistivity) versus inverse absolute temperature during heating are shown in *Fig. 7*. From the slope (negative) of the Arrhenius plot, which is quite linear, the activation energy can be calculated. The linearity of the Arrhenius plot means that the activation energy does not change throughout the temperature variation. This activation energy is the energy for electron jumping from one lamina to the other. Electronic excitation across this energy enables conduction in the through-thickness direction.

The activation energies, thicknesses and room temperature contact resistivities for samples made at different curing pressures and composite configurations are shown in *Table 1*. All the activation energies were calculated based on the data at 75–125°C. In this temperature regime, the temperature change was

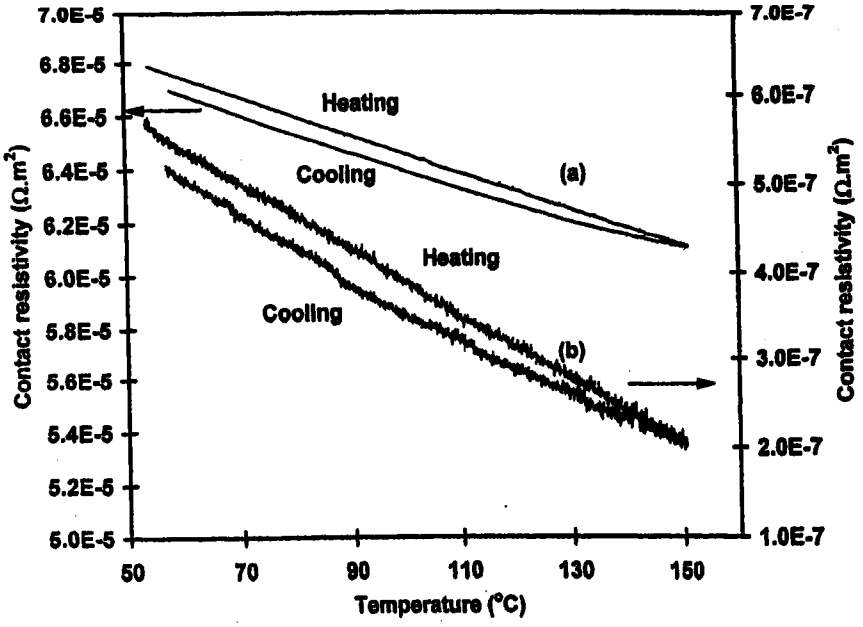

Fig. 6. Variation of contact electrical resistivity with temperature during heating and cooling of carbon fiber epoxy-matrix composites at 0.15°C/min (a) for composite made without any curing pressure and (b) for composite made with a curing pressure 0.33 MPa.

Table 1. Activation Energy for Various Carbon Fiber Epoxy-Matrix Composites. The Standard Deviations Are Shown in Parentheses.

Composite Configuration	Curing Pressure (MPa)	Composite Thickness (mm)	Contact Resistivity ρ_{co} ($\Omega.m^2$)	Activation energy (kJ/mol) Heating at 0.15°C/min	Heating at 1°C/min	Cooling at 0.15°C/min
Crossply	0	0.36	7.3×10^{-5}	1.26 (2×10^{-3})	1.24 (3×10^{-3})	1.21 (8×10^{-4})
	0.062	0.32	1.4×10^{-5}	1.26 (4×10^{-3})	1.23 (7×10^{-3})	1.23 (4×10^{-3})
	0.13	0.31	1.8×10^{-5}	1.62 (3×10^{-3})	1.57 (4×10^{-3})	1.55 (2×10^{-3})
	0.19	0.29	5.4×10^{-6}	2.14 (3×10^{-3})	2.15 (3×10^{-3})	2.13 (1×10^{-3})
	0.33	0.26	4.0×10^{-7}	11.4 (4×10^{-2})	12.4 (8×10^{-2})	11.3 (3×10^{-2})
Unidirectional	0.42	0.23	2.9×10^{-5}	1.02 (3×10^{-3})	0.82 (4×10^{-3})	0.78 (2×10^{-3})

very linear and well controlled. From *Table 1* it can be seen that, for the same composite configuration (crossply), the higher the curing pressure, the smaller the composite thickness (because of more epoxy being squeezed out), the lower the contact resistivity, and the higher was the activation energy. A smaller composite thickness corresponds to a higher fiber volume fraction in the composite. During curing and subsequent cooling, the matrix shrinks, so a longitudinal compressive stress will develop in the fibers. For carbon fibers, the modulus in the longitudinal direction is much higher than that in the transverse direction. Moreover, the carbon fibers are continuous in the longitudinal direction. Thus, the overall shrinkage in the longitudinal direction tends to be less than that in the transverse direction. Therefore, there will be a residual interlaminar stress in the two crossply layers in a given direction. This stress accentuates the barrier for the electrons to jump from one lamina to the other. After curing and subsequent cooling, heating will decrease the thermal stress. Both the thermal stress and the curing stress contribute to the residual interlaminar stress. Therefore, the higher the curing pressure, the larger the fiber volume fraction, the greater the residual interlaminar stress, and the higher was the activation energy, as shown in *Table 1*. Besides the residual stress, thermal expansion can also affect contact resistance by changing the contact area. However, calculation shows that the contribution of thermal expansion is less than one-tenth of the observed change in contact resistance with temperature.

The electron jump primarily occurs at points where direct contact occurs between fibers of the adjacent laminae. The direct contact is possible due to the flow of the epoxy resin during composite fabrication and due to the slight waviness of the fibers, as explained in Ref. 49 in relation to the through-thickness volume resistivity of a carbon fiber epoxy-matrix composite.

The curing pressure for the sample in the unidirectional composite configuration was higher than that of any of the crossply samples (*Table 1*). Consequently, the thickness was the lowest. As a result, the fiber volume fraction was the highest. However, the contact resistivity of the unidirectional sample was the second highest rather than being the lowest, and its activation energy was the lowest rather than the highest. The low activation energy is consistent with the fact that there was no CTE or curing shrinkage mismatch between the two unidirectional laminae and, as a result, no interlaminar stress between the laminae. This low value supports the notion that the interlaminar stress is important in affecting the activation energy. The high contact resistivity for the unidirectional case can be explained in the following way. In the crossply samples, the pressure during curing forced the fibers of the two laminae to press on to one another and hence contact tightly. In the unidirectional sample, the fibers of one of the laminae just sank into the other lamina at the junction, so pressure helped relatively little in the contact between fibers of adjacent laminae. Moreover, in the crossply situation, every fiber at the lamina-lamina interface contacted many fibers of the other lamina, while, in the unidirectional situation, every fiber had little chance to contact the fibers of the other lamina. Therefore, the number of contact points between the two laminae was less for the unidirectional sample than the crossply samples.

TEMPERATURE EFFECTS (SEEBECK EFFECT)

The thermocouple function stems from the use of dissimilar (preferably n-type and p-type) carbon fibers (as obtained by intercalation) in different laminae. The thermocouple sensitivity and linearity are as good as or better than those of commercial thermocouples. By using two laminae in a crossply orientation, a two-dimensional array of thermistors (last section) or thermocouple (this section) junctions are obtained, thus allowing temperature distribution sensing.

Table 2 shows the Seebeck coefficient and the absolute thermoelectric power of carbon fibers and the

Table 2. Seebeck Coefficient (μV/°C) and Absolute Thermoelectric Power (μV/°C) of Carbon Fibers and Thermocouple Sensitivity (μV/°C) of Epoxy-Matrix Composite Junctions. All Junctions Are Unidirectional Unless Specified as Crossply. The Temperature Range is 20–110°C.

	Seebeck coefficient with copper as the reference (μV/°C)	Absolute thermoelectric power (μV/°C)	Thermocouple sensitivity (μV/°C)
P-25*	–0.8	+1.5	
T-300*	+5.0	+7.3	
P-25* + T-300*			+5.5
P-25* + T-300* (crossply)			+5.4
P-100*	+1.7	+4.0	
P-120*	+3.2	+5.5	
P-100 (Na)	+48	+50	
P-100 (Br_2)	–43	–41	
P-100 (Br_2) + P-100 (Na)			+82
P-120 (Na)	+42	+44	
P-120 (Br_2)	–38	–36	
P-120 (Br_2) + P-120 (Na)			+74

*Pristine (i.e., not intercalated).

thermocouple sensitivity of epoxy-matrix composite junctions. A negative value of the absolute thermoelectric power indicates p-type behavior; a positive value indicates n-type behavior. Pristine P-25 is slightly n-type; pristine T-300 is strongly n-type. A junction comprising pristine P-25 and pristine T-300 has a positive thermocouple sensitivity that is close to the difference of the Seebeck coefficients (or the absolute thermoelectric powers) of T-300 and P-25, whether the junction is unidirectional or crossply. Pristine P-100 and pristine P-120 are both slightly n-type. Intercalation with sodium causes P-100 and P-120 to become strongly n-type. Intercalation with bromine causes P-100 and P-120 to become strongly p-type. A junction comprising bromine intercalated P-100 and sodium intercalated P-100 has a positive thermocouple sensitivity that is close to the sum of the magnitudes of the absolute thermoelectric powers of the bromine intercalated P-100 and the sodium intercalated P-100. Similarly, a junction comprising bromine intercalated P-120 and sodium intercalated P-120 has a positive thermocouple sensitivity that is close to the sum of the magnitudes of the absolute thermoelectric powers of the bromine intercalated P-120 and the sodium intercalated P-120. *Figure 8* shows the linear relationship of the measured voltage

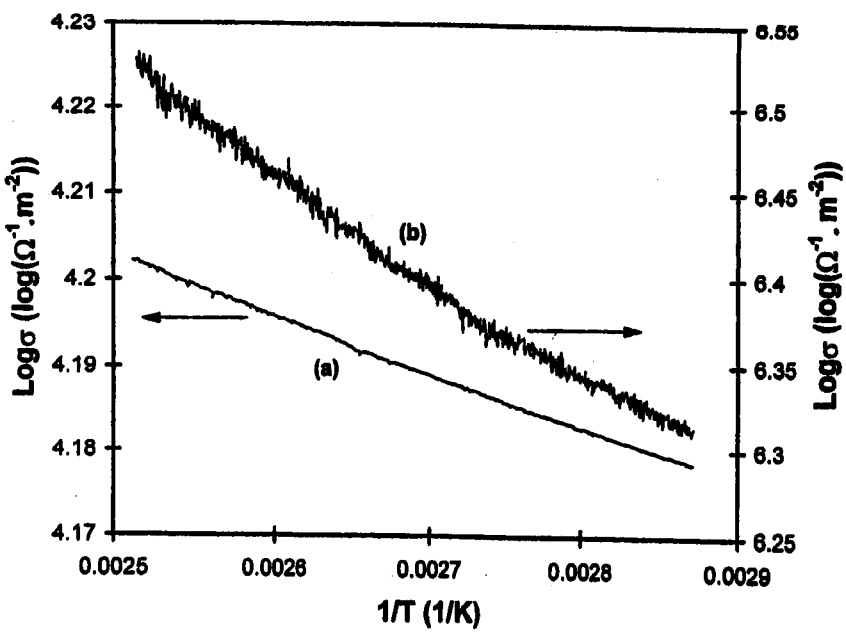

Fig. 7. Arrhenius plot of log contact conductivity vs. inverse absolute temperature during heating of carbon fiber epoxy-matrix composites at 0.15°C/min (a) for composite made without any curing pressure and (b) for composite made with curing pressure 0.33 MPa.

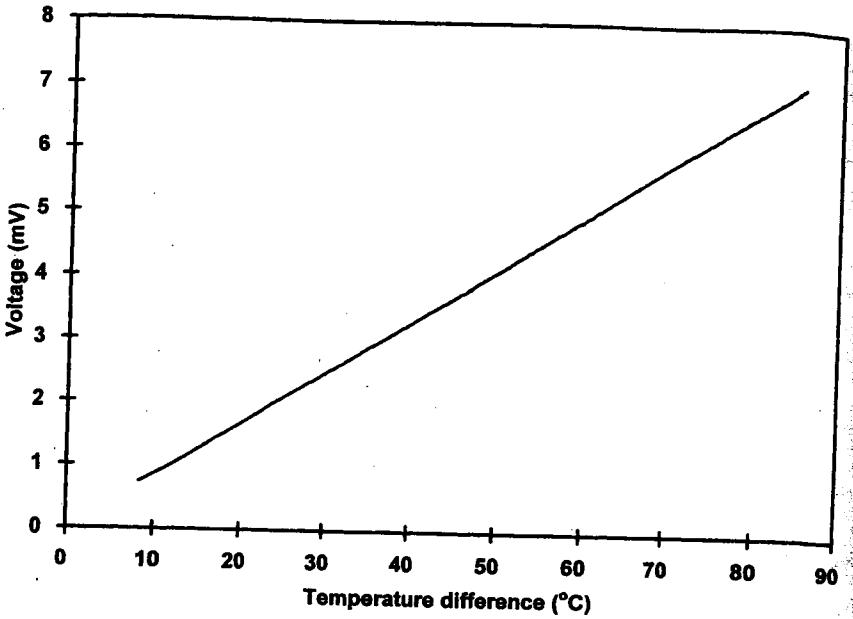

Fig. 8. Variation of the measured voltage with the temperature difference between hot and cold points for the carbon fiber epoxy-matrix composite junction comprising bromine intercalated P-100 and sodium intercalated P-100 carbon fibers.

with the temperature difference between hot and cold points for the junction comprising bromine intercalated P-100 and sodium intercalated P-100. In *Fig. 8*, the data points are so numerous that they cannot be distinguished along the curve.

A junction comprising n-type and p-type partners has a thermocouple sensitivity that is close to the sum of the magnitudes of the absolute thermoelectric powers of the two partners. This is because the electrons in the n-type partner as well as the holes in the p-type partner move away from the hot point toward the corresponding cold point. As a result, the overall effect on the voltage difference between the two cold ends is additive.

By using junctions comprising strongly n-type and strongly p-type partners, a thermocouple sensitivity as high as +82 μV/°C was attained. Semiconductors are known to exhibit much higher values of the Seebeck coefficient than metals, but the need to have thermocouples in the form of long wires makes metals the main materials for thermocouples. Intercalated carbon fibers exhibit much higher values of the Seebeck coefficient than metals. Yet, unlike semiconductors, their fiber form and fiber composite form make them convenient for practical use as thermocouples.

The thermocouple sensitivity of the carbon fiber epoxy-matrix composite junctions is independent of the extent of curing and is the same for unidirectional and crossply junctions. This is consistent with the fact that the thermocouple effect hinges on the difference in the bulk properties of the two partners, and is not an interfacial phenomenon. This behavior means that the interlaminar interfaces in a fibrous composite serve as thermocouple junctions in the same way, irrespective of the lay-up configuration of the dissimilar fibers in the laminate. As a structural composite typically has fibers in multiple directions, this behavior facilitates the use of a structural composite as a thermocouple array.

It is important to note that the thermocouple junctions do not require any bonding agent other than the epoxy, which serves as the matrix of the composite and does not serve as an electrical contact medium (since it is not conducting). In spite of the presence of the epoxy matrix in the junction area, direct contact occurs between a fraction of the fibers of a lamina and a fraction of the fibers of the other lamina, thus resulting in a conduction path in the direction perpendicular to the junction (11).

APPARENT NEGATIVE ELECTRICAL RESISTANCE

Electrical resistance is the slope of the voltage-current curve. If this slope is negative, the resistance, at least apparently, is negative. This kind of resistance is referred to as apparent negative resistance (37). *Figure 9a* shows a typical current-voltage characteristic for a sample cured at 0.13 MPa. It is quite linear and has a positive slope. *Figure 9b* shows that for a sample cured at 1.4 MPa. It is also quite linear but has a negative slope. For an intermediate curing pressure of 0.33 MPa, two types of current-voltage characteristics were observed (*Fig. 10*). The deviation from linearity in *Fig. 10* is such that the apparent resistance becomes more negative or less positive when the current is high, probably due to the enhancement of the drift current.

The apparent contact resistivities for different current directions and curing pressures are shown in *Table 3*. It can be seen that the apparent contact resistivities for the sample with the lowest curing pressure (0.13 MPa)

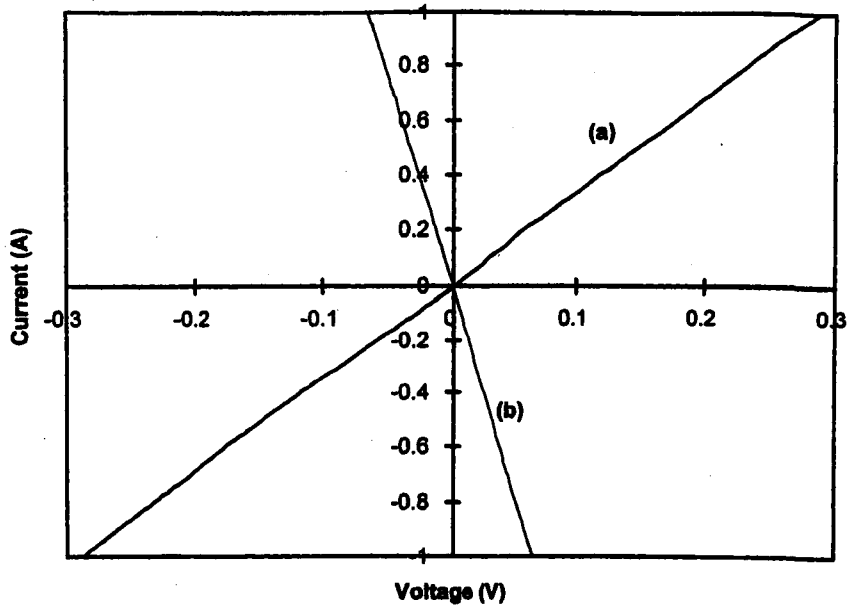

Fig. 9. Typical current-voltage characteristics for carbon fiber epoxy-matrix composite cured at (a) 0.13 MPa (thick line), (b) 1.4 MPa (thin line).

are all positive, those for the sample with the highest curing pressure (1.4 MPa) are all negative, and those for the sample with the intermediate curing pressure (0.33 MPa) are partly positive (in the A-C and B-D directions) and partly negative (in the A-D and B-C directions). These behaviors are consistent with *Fig. 9* and *10*.

Another interesting fact from *Table 3* is that, for the samples cured at 1.4 and 0.33 MPa, the apparent contact resistivities in the A-C and B-D directions are quite close and those in the A-D and B-C directions are also quite close, whereas the resistivities in the A-C (or B-D) and B-C (or A-D) directions are quite different. For the sample cured at 0.13 MPa, all four resistivities are close. *Table 3* also shows the thickness of each two-lamina composite. Half of this thickness is the thickness of a lamina. For the samples cured at 1.4 and 0.33 MPa, a more negative apparent resistivity is associated with a lower thickness of the composite at the corner (quadrant) of the junction close to the current contacts; the thicknesses were measured by a micrometer. A lower local thickness is probably caused by the flow of epoxy during curing. Hence, the variation of the resistivity with the current direction is attributed to non-uniformity in the thickness within a junction. A low thickness favors an apparent negative resistance, akin to a high curing pressure favoring an apparent negative resistance. For a low curing pressure

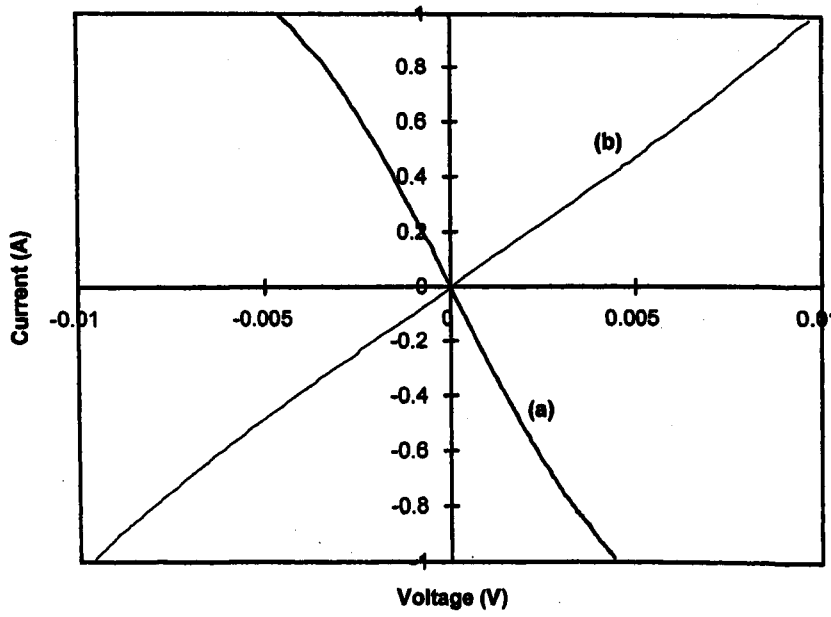

Fig. 10. Two types of current-voltage characteristics for carbon fiber epoxy-matrix composite cured at 0.33 MPa. (a) Negative slope (thick line). (b) Positive slope (thin line).

Table 3. The Relationships Among Apparent Contact Resistivity, Curing Pressure and Current Direction for Carbon Fiber Epoxy-Matrix Composites.

Curing Pressure (MPa)	Thickness at center (mm)	Direction of current (See *Fig. 1a*)	Thickness at corner* (mm)	Apparent contact resistivity ($\Omega.m^2$)	Current range for resistivity calculation (A)
1.4	0.236	A to C	0.246	-4.23×10^{-6}	0–1
		A to D	0.234	-4.87×10^{-6}	0–1
		B to C	0.226	-4.83×10^{-6}	0–1
		B to D	0.226	-4.25×10^{-6}	0–1
0.33	0.284	A to C	0.284	5.11×10^{-7}	0–0.4
		A to D	0.274	-1.87×10^{-7}	0–0.4
		B to C	0.277	-2.68×10^{-7}	0–0.4
		B to D	0.282	5.32×10^{-7}	0–0.4
0.13	0.315	A to C	0.325	1.21×10^{-5}	0–1
		A to D	0.310	1.21×10^{-5}	0–1
		B to C	0.307	1.25×10^{-5}	0–1
		B to D	0.269	1.20×10^{-5}	0–1

*"Corner" refers to the quadrant of the square junction that is closest to both current contacts, which are A and C, A and D, B and C, or B and D.

(the 0.13 MPa case), the flow of epoxy is probably less and a positive resistance apparently depends on thickness less than an apparent negative resistance, so the resistivity does not vary with the current direction.

Figure 11 (37) shows the resistance (with the current from A to C) of a junction at a constant pressure of 1.4 MPa during curing. The apparent resistance is negative throughout the curing process, though it becomes more negative as the temperature increases toward the curing temperature. After curing and subsequent cooling, the apparent resistances are –0.0297, –0.0306, –0.0309 and –0.0296 Ω in the AC, AD, BC and BD directions respectively. As in *Table 3*, two of these resistances (AC and BD) are close, and the other two (AD and BC) are also close. Though the absolute value of these resistances vary from sample to sample, that all four resistances are negative and that two (AC and BD) are close and the other two (AD and BC) are close is behavior observed in every sample with two crossply laminae cured at 1.4 MPa.

For a two-lamina sample, the measured resistance in the through-thickness direction is the apparent contact resistance of one interlaminar interface. For a three-lamina sample, the through-thickness resistance is the sum of the apparent contact resistances of the two interlaminar interfaces and the volume resistance in the through-thickness direction of one lamina. Thus, by having more than two laminae, the apparent negative resistance due to the contact resistance and the positive resistance due to the volume resistance are in series.

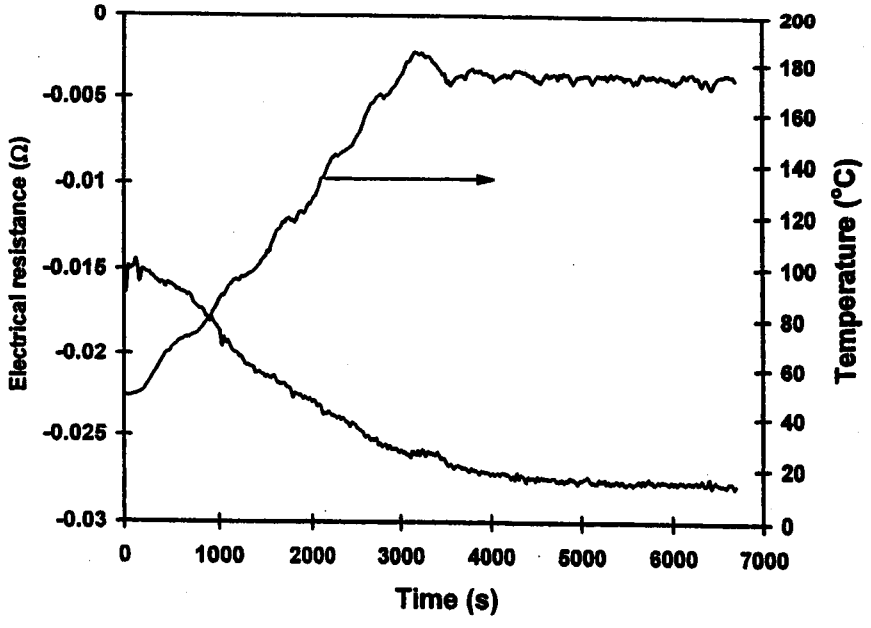

Fig. 11. Variation of resistance during curing at 1.4 MPa of a two-lamina crossply carbon fiber epoxy-matrix composite.

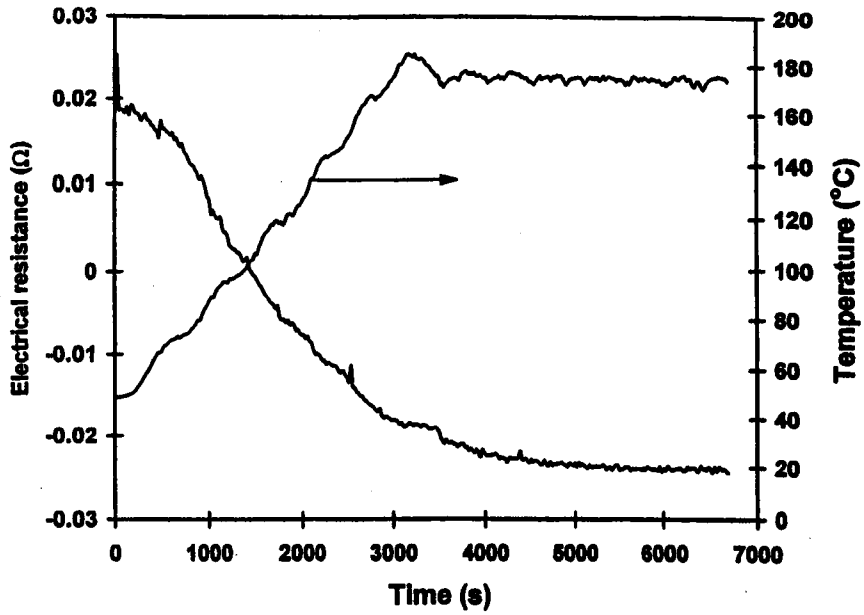

Fig. 12. Variation of resistance during curing at 1.4 MPa of a four-lamina crossply carbon fiber epoxy-matrix composite.

Four laminae stacked in a crossply (0/90/0/90) configuration were subjected to a pressure of 1.4 MPa during curing. Since the volume resistance within each lamina in the through-thickness direction is positive, the total (series) through-thickness apparent resistance of the stack [*Fig. 12* (37)] is not as negative as a single interlaminar junction (*Fig. 11*). At the beginning of the heating of the stack, the apparent resistance is positive. As the temperature increases, it becomes less positive, goes through zero and then becomes negative. After curing and subsequent cooling, it remains negative, at –0.0261, –0.0087, –0.0090 and –0.0262 Ω for current directions AC, AD, BC and BD respectively.

Three laminae stacked in a crossply (0/90/0) configuration were within the four-lamina stack mentioned above. After curing at 1.4 MPa and subsequent cooling, the through-thickness apparent resistances of the three-lamina stack are +0.0007, –0.0771, –0.0771 and +0.0007 Ω for the four directions of current flow (37). In another three-lamina stack within the four-lamina stack mentioned above, the apparent resistances after 1.4 MPa curing and cooling are +0.0024, –0.0713, –0.0712 and +0.0024 Ω for the four directions of current flow (37). Thus, by tailoring the stack and using the appropriate direction of current flow, the apparent resistance can be close to zero (e.g, +0.0007 Ω). Another way to attain apparent zero resistance is to adjust the curing pressure, as suggested by *Table 3*.

A mechanism for the apparent negative resistance, as suggested by the experimental results, is given below. Upon application of a current from A to C (positive end of the applied voltage at A, the top lamina) between two crossply laminae, electrons drift from the bottom lamina to the top lamina through the fiber-fiber contacts, though the drift requires the jumping of electrons across the interface between the laminae through activation to overcome the associated energy barrier. After jumping across the interface through drift, the electrons may travel along the top lamina away from the AC quadrant of the interface that is exposed most strongly to the applied current and then, due to entropy (i.e., diffusion), flow back to the bottom lamina at the fiber-fiber contacts. The backflow current overshadows the drift current in its influence on the measured voltage between B and D, because the backflow occurs away from the AC quadrant, mainly at the BD quadrant. Therefore, the measured voltage corresponds to the electrons going from top to bottom laminae, or, in other words, down the applied voltage gradient. The drift of the electrons up the voltage gradient is necessary to supply the electrons which subsequently flow back. Consequently, the greater the voltage gradient, the greater the drift current and hence the greater the backflow current. Therefore, though backflow itself does not require a voltage gradient, the backflow current increases with the voltage gradient. The free energy that drives the backflow current is derived from the energy of the drift current and the entropy increase associated with the backflow.

If the curing pressure during composite fabrication is not high enough, there are not enough fiber-fiber contacts, so the electrons spread out at the bottom lamina at the interface and drift across the entire interface to the top lamina. As a result, there is no backflow current and the measured voltage is positive, corresponding to a positive resistance. If the epoxy matrix is replaced by a thermoplastic (PPS) matrix, the amount of fiber-fiber contacts is insufficient for the occurrence of apparent negative resistance.

For a four-lamina stack exhibiting an apparent zero resistance, the apparent zero resistance is due to the balance between the backflow current and the forward flowing current in the quadrant near the voltage probes.

EFFECTS OF GLASS TRANSITION AND MELTING OF THE POLYMER MATRIX

The glass transition and melting behavior of a thermoplastic polymer depends on the degree of crystallinity, the crystalline perfection and other factors (38–43). Knowledge of this behavior is valuable for the processing and use of the polymer. This behavior is most commonly studied by differential scanning calorimetry (DSC) (38–43), although the DSC technique is limited to small samples and the associated equipment is expensive and not portable. As the degree of crystallinity and the crystalline perfection of a polymer depend on the prior processing of the polymer and the effect of a process on the microstructure depends on the size and geometry of the polymer specimen, it is desirable to test the actual piece (instead of a small specimen) for the glass transition and melting behavior.

DSC is a thermal analysis technique for recording the heat necessary to establish a zero temperature difference between a small specimen and a reference material, which are subjected to identical temperature programs in an environment heated or cooled at a controlled rate (44). The recorded heat flow gives a measure of the amount of energy absorbed or evolved in a particular physical or chemical transformation, such as the glass transition, melting or crystallization. The concept here is totally different from that of DSC. This technique involves measuring the DC electrical resistance when the polymer has been reinforced with electrically conducting fibers such as continuous carbon fibers. The resistance is in the fiber direction. The polymer molecular movements that occur at the glass transition and melting disturb the carbon fibers, which are much more conducting than the polymer matrix, and affect the electrical resistance of the composite in the fiber direction, thereby allowing the resistance change to indicate the glass transition and melting behavior. The resistance measurement can be performed on large pieces of composite and the electronic equipment (a multimeter) involved is simple and portable. Thus, this technique is expected to be useful for the testing of composite parts in the process of fabrication as well as during use.

Exposure of polyamides to heat and oxygen may cause changes in the physical and chemical characteristics due to thermal oxidative degradation (45) and thus changes in the mechanical properties. Prolonged annealing at a high temperature results in undesirable changes in the degree of crystallization and in the end groups, and may cause inter- and intramolecular transamidation reactions, chain scission and crosslinking (46–51). The capability of the electrical resistance technique has been shown (52) by studying the effect of annealing in air at various temperatures below the melting temperature for various lengths of time on the glass transition and melting behavior of Nylon-6 thermoplastic polymer reinforced with unidirectional continuous carbon fibers (Nylon-6/CF).

Figure 13a (52) shows the fractional change in resistance for the as-received composite during heating, in which the temperature was raised from 25 to 350°C at a rate of 0.5°C/min. Two peaks were observed. The onset temperature of the first peak was 80°C and that of the second peak was 220°C. The first peak is attributed to matrix molecular movement above T_g; the second peak is attributed to matrix molecular movement above T_m. Because the molecular movement above T_g is less drastic than that above T_m, the first peak is much lower than the second one. The DSC thermogram of the as-received composite does not show a clear glass transition [*Fig. 14a* (52)]. Therefore, the resistance is more sensitive to the glass transition than DSC. The onset temperature (220°C) of the second peak (*Fig. 13a*) is higher than the onset temperature (T_{onset} = 200.9°C) of the DSC melting peak (*Fig. 14a*) and is close to the melting temperature (T_m = 218.5°C) indicated by DSC (*Fig. 14a*). The matrix molecular movement at T_{onset} is less intense than that at T_m, thereby giving no effect on the resistance curve at T_{onset}. Another reason may be a time lag between the matrix molecular movement and the resistance change.

Figure 13b, *13c* and *13d* show the effect of the annealing temperature. Comparison of *Fig. 13a* and *13b* shows that annealing at 100°C for 5 h (*Fig. 13b*) had little effect on the glass transition and melting behavior of the Nylon-6 matrix; this is consistent with the DSC results (*Fig. 14a* and *14b*). When the annealing temperature increased to 180°C (*Fig. 13c*), the peak due to molecular movement above T_g disappeared. This is attributed to the increase of the degree of crystallinity due to annealing. Because the crystalline portion has constraint on the molecule mobility, the higher the degree of crystallinity, the less is the possibility of molecular movement above T_g.

Not only does the degree of crystallinity but also the extent of thermal degradation affects the molecule mobility above T_g. *Figure 13d* shows the fractional change in resistance of the sample annealed at 200°C for 5 h. No peak due to molecular movement above T_g was observed. The degree of crystallinity was less than that of the as-received sample, as shown by the enthalpy change (ΔH) in *Table 4* (52). However the higher extent of thermal degradation resulted in less molecular movement above T_g.

Figure 13c and *13e* show the effect of annealing time from 5 to 15 h at 180°C. The height of the peak due to molecular movement above T_m decreased as the annealing time increased. A longer annealing time resulted in a higher extent of thermal degradation of the matrix, which retarded the molecular movement above T_m. That this effect is due to a change of the thermal degradation is also supported by the effect of annealing temperature, as shown in *Fig. 13c* and *13d*. A higher annealing temperature likely enhanced the extent of thermal degradation, thus resulting in a decrease of the height of the peak associated with molecular movement above T_m. Since the tail is more

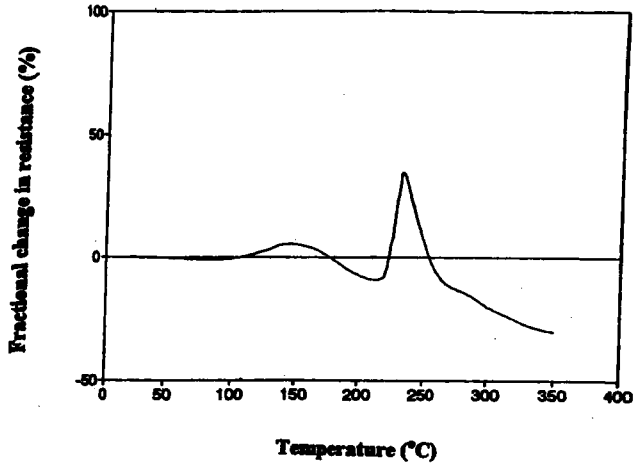

(a)

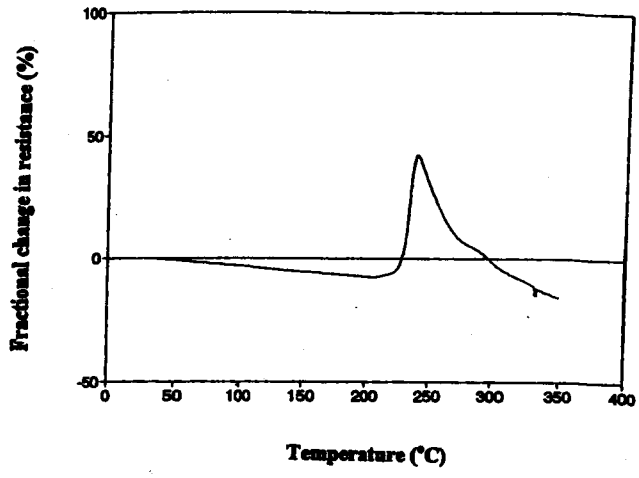

(d)

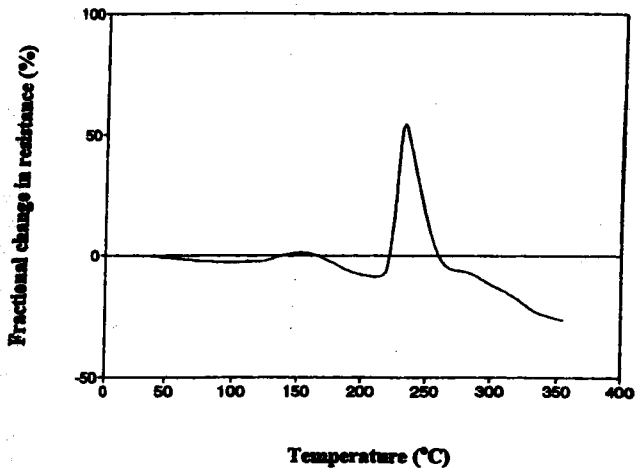

(b)

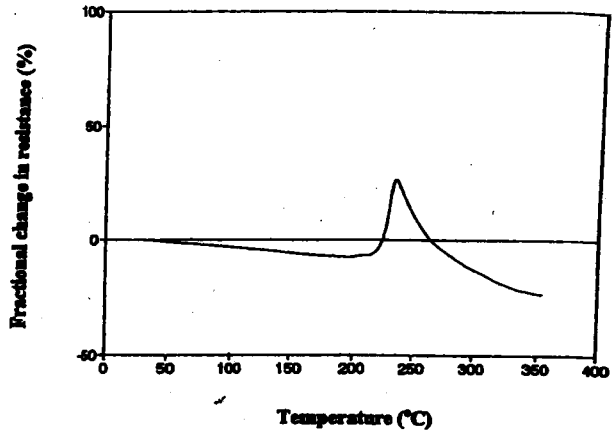

(e)

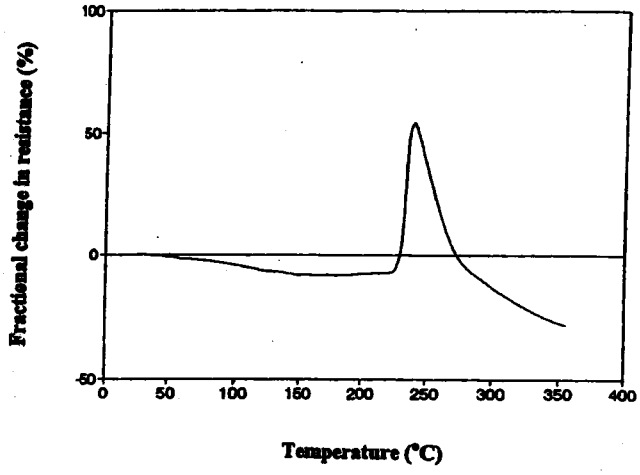

(c)

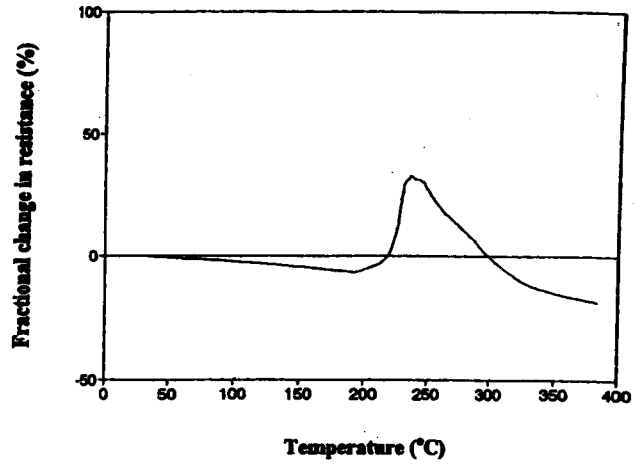

(f)

Fig. 13. Effect of annealing condition on the variation of the electrical resistance with temperature for a carbon fiber thermoplastic (Nylon-6) matrix composite. a. As-received; b. 100°C, 5 h.; c. 180°C, 5 h.; d. 200°C, 5 h.; e. 180°C, 15 h.; f. 180°C, 30 h.

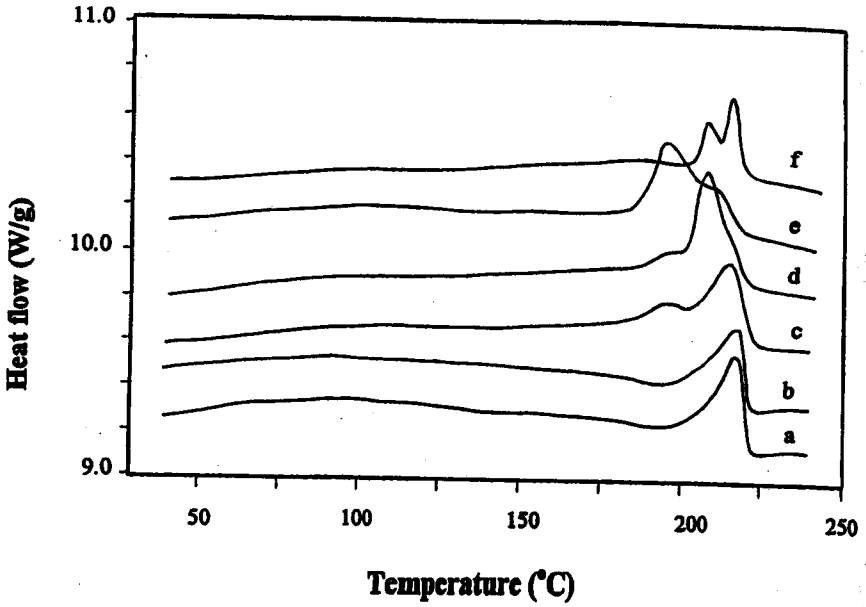

Fig. 14. DSC thermograms showing the melting endothermic peaks before and after annealing at the temperatures and for the times shown for a carbon fiber thermoplastic (Nylon-6) matrix composite. a. As-received.; b. 100°C , 5 h.; c. 180°C, 5 h.; d. 180°C, 15 h.; e. 180°C, 30 h.; f. 200°C, 5 h.

pronounced for samples with a higher extent of thermal degradation, as shown in *Fig. 13d* and *13f*, it may be attributed to the lower molecular mobility due to extensive thermal degradation.

COMPOSITE-COMPOSITE JOINTS BY ADHESION

Bonding

The joining of materials is important for manufacturing and repair of composite material products. Joining methods for polymers and polymer-matrix composites include fusion bonding, diffusion bonding (or autohesion), use of adhesives, and fastening. In particular, autohesion is relevant to the self-healing of polymers. Diffusion bonding (or autohesion) involves interdiffusion between the adjoining materials in the solid state. In contrast, fusion bonding involves melting. Due to the relatively low temperatures of diffusion bonding compared to fusion bonding, diffusion bonding does not suffer from the undesirable side effects that typically occur in fusion bonding, such as degradation and crosslinking of the polymer matrix. Although the diffusion bonding of metals has been widely studied (53–57), relatively little study has been conducted on the autohesion of polymers (58–73). Because of the increased segment mobility above the glass transition temperature (T_g), thermoplastics are able to undergo interdiffusion above T_g.

Diffusion, as a thermally activated process, takes time. In other words, how long diffusion takes depends on the temperature. In order for diffusion bonding or autohesion to be conducted properly, the kinetics of the process needs to be known.

The study of the kinetics requires monitoring the process as it occurs. A real-time monitoring technique

Table 4. Calorimetry Data for Carbon Fiber Nylon-6 Composite Before and After Annealing.

Annealing Condition					
Temperature (°C)	Time (h)	T_{ml}[a] (°C)	T_{onset}[b] (°C)	T_m[c] (°C)	ΔH[d] (J/g)
[e]	[e]		200.9	218.5	26.7
100	5		205.5	218.2	26.6
180	5	194.8	201.3	215.5	34.8
180	15	196.3	201.4	208.9	39.1
180	30	196.3	200.0	209.0	38.6
200	5	208.3	212.9	216.4	16.5

[a]Peak temperature of the low-temperature melting peak.
[b]Onset temperature of the high-temperature melting peak.
[c]Peak temperature of the high-temperature melting peak.
[d]Heat of fusion.
[e]As-received.

is obviously preferable to a traditional method that requires periodic interruption and cooling of the specimen. However, real-time monitoring is experimentally difficult compared with interrupted monitoring. The method described here is ideal for thermoplastic prepregs containing continuous carbon fibers, since the carbon fibers are conductive. Two carbon-fiber thermoplastic prepreg plies are placed together to form a joint. The electrical contact resistance of this joint is measured during autohesion. As autohesion occurs, the fibers in the plies undergoing joining come closer together, thus resulting in a decrease in the contact resistance. Hence, with the measurement of this resistance in real time, the autohesion process was monitored as a function of time at different selected bonding temperatures for Nylon-6 and polyphenylenesulfide (PPS), both thermoplastics (74). Arrhenius plots of a characteristic resistance decrease versus temperature allows determination of the activation energy for the process. This method can possibly be used for monitoring of bonding of unfilled thermoplastics if a few carbon fibers are strategically placed.

Debonding

Engineering thermoplastics can be bonded together by solid state welding (i.e., interdiffusion or autohesion above the glass transition temperature but below the melting temperature) or fusion welding (i.e., melting and subsequent solidification). Both methods involve heating and subsequent cooling. During cooling, the thermoplastic goes from a soft solid state (in the case of solid state welding) or a liquid state (in the case of fusion welding) to a stiff state. If the thermoplastic members to be joined are anisotropic (as in the case of each member being reinforced with fibers) and the fiber orientation in the two members is not the same, the thermal expansion (actually contraction) mismatch at the bonding plane will cause thermal stress to build up during cooling. This thermal stress is detrimental to the quality of the adhesive bond formed between the two members.

Two scenarios can lead to the absence of bonding after cooling. One scenario is the absence of bond formation at the high temperature during welding, due to insufficient time or temperature. The other scenario is the presence of bonding at the high temperature, but the occurrence of debonding during subsequent cooling due to thermal stress. The cause of the absence of bonding is different in the two scenarios. In any given situation, the cause of the debonded joint must be understood if the absence of bonding after cooling is to be avoided.

The propensity for mutual diffusion in thermoplastic polymers increases with temperature. The contact at the interface across which interdiffusion takes place also plays a role. An intimate interface, as obtained by application of pressure to compress the two members together, also facilitates diffusion. Thus, the quality of the joint improves with increasing temperature and increasing pressure in the high temperature period of welding. The poorer is the quality of the joint attained at a high temperature, the greater is the likelihood that thermal stress built up during subsequent cooling will be sufficient to cause debonding. Hence, merely having bonding achieved at the high temperature in welding is not enough. The bond achieved must be of sufficient quality to withstand the abuse of thermal stress during subsequent cooling.

The quality of a joint is conventionally tested destructively by mechanical methods or nondestructively by ultrasonic methods (75, 76). This testing is performed at room temperature after the joint has been cooled from the high temperature used in welding. As a result, the testing does not allow distinction between the two scenarios described above. The use of a nondestructive method, namely contact electrical resistance measurement, to monitor joint quality in real time during the high temperature period of welding and also during subsequent cooling has been shown (77). The resistance increased by up to 600% upon debonding. The resistance increase was much greater than the resistance decrease during prior bonding. Debonding occurred during cooling when the pressure or temperature during prior bonding was not sufficiently high.

Adhesive joint formation between thermoplastic adherends typically involves heating to temperatures above the melting temperature (T_m) of the thermoplastic. During heating to the desired elevated temperature, time is spent in the range between the glass transition temperature (T_g) and the T_m. The dependence of the bond quality on the heating rate, heating time, and pressure was investigated through measurement of the contact resistance between adherends in the form of carbon fiber reinforced PPS (78). A long heating time below the melting temperature (T_m) was found to be detrimental to subsequent PPS adhesive joint development above T_m. This is due to curing reactions below T_m and consequent reduced mass flow response above T_m. A high heating rate (small heating time) enhanced the bonding more than a high pressure.

COMPOSITE-COMPOSITE JOINTS BY FASTENING

Mechanical fastening is one of the most common methods of joining. It involves the application of a force to the components to be jointed. Examples of fasteners are rivets, bolts, screws and nuts. Fasteners as well as components are most commonly made of metals, such as steel. However, polymers are increasingly used for both fasteners and components, due to their moldability, low density and corrosion resistance.

Due to the electrically insulating behavior of conventional polymers and the need for an electrical conductor for the purpose of measuring the contact electrical

resistance, a polymer that contained continuous carbon fibers in a direction parallel to the plane of the joint was used (79). The carbon fibers caused the composite to be electrical conducting in the fiber direction, as well as the through-thickness direction, because there is some degree of contact between adjacent fibers in the composite in spite of the presence of the matrix (11). Due to the direction of the fibers, the mechanical properties of the composite in the through-thickness direction are dominated by the polymer matrix, as desired for studying a mechanically fastened polymer-polymer joint.

Contact resistance measurement was used to investigate the effect of repeated fastening and unfastening on a polymer-polymer joint interface (79). A polymer-polymer joint obtained by mechanical fastening at a compressive stress of 5% (or less) of the 1% offset yield strength of the polymer (Nylon-6) was found to exhibit irreversible decrease in the contact electrical resistance upon repeated fastening (loading) and unfastening (unloading). The decrease occurred after up to 10 cycles of fastening and unfastening, although the decrease diminished with cycling. It is primarily due to local plastic deformation of the matrix at the asperities at the interface. Moreover, the stress required for the resistance to reach its minimum in a cycle decreased with cycling, due to softening of the matrix.

COMPOSITE-CONCRETE JOINTS BY ADHESION

Continuous fiber polymer-matrix composites are increasingly used to retrofit concrete structures, particularly columns (80–92). The retrofit involves wrapping a fiber sheet around a concrete column or placing a sheet on the surface of a concrete structure, such that the fiber sheet is adhered to the underlying concrete by using a polymer, most commonly epoxy. This method is effective for the repair of even quite badly damaged concrete structures. Although the fibers and polymer are very expensive compared to concrete, the alternative of tearing down and rebuilding the concrete structure is often even more expensive than the composite retrofit. Both glass fibers and carbon fibers are used for the composite retrofit. Glass fibers are advantageous for their relatively low cost, but carbon fibers are advantageous for their high tensile modulus.

The effectiveness of a composite retrofit depends on the quality of the bond between the composite and the underlying concrete, as good bonding is necessary for load transfer. Peel testing for bond quality evaluation is destructive (93). Nondestructive methods to evaluate the bond quality are valuable. They include acoustic methods, which are not sensitive to small amount of debonding or bond degradation (94), and dynamic mechanical testing (95). Electrical resistance measurement was used for nondestructive evaluation of the interface between concrete and its carbon fiber composite retrofit (96). The method was effective for studying the effects of temperature and debonding stress on the interface. The concept behind the method is that bond degradation causes the electrical contact between the carbon fiber composite retrofit and the underlying concrete to degrade. Since concrete is electrically more conducting than air, the presence of an air pocket at the interface causes the measured apparent volume resistance of the composite retrofit in a direction in the plane of the interface to increase. Hence, bond degradation is accompanied by an increase in the apparent resistance of the composite retrofit. Although the polymer matrix (epoxy) is electrically insulating, the presence of a thin layer of epoxy at the interface was unable to electrically isolate the composite retrofit from the underlying concrete.

The apparent resistance of the retrofit in the fiber direction was increased by bond degradation, whether the degradation was due to heat or stress. The degradation was reversible. Irreversible disturbance in the fiber arrangement occurred slightly as thermal or load cycling occurred, as indicated by the resistance decreasing cycle by cycle (96).

CONCLUSION

DC electrical measurements are effective for studying continuous carbon fiber polymer-matrix composites in terms of their microstructure, strain effects, damage effects and temperature effects, as well as their joints obtained by adhesion or fastening.

Tensile strain in the longitudinal direction causes the longitudinal resistance to decrease reversibly and the through-thickness resistance to increase reversibly, due to increase in the degree of fiber alignment. Compressive strain in the longitudinal direction causes the reverse effects. Damage in the form of delamination causes the through-thickness resistance to increase irreversibly. Damage in the form of fiber breakage causes the longitudinal resistance to increase irreversibly. Increase in temperature causes the contact resistance between laminae to increase reversibly, particularly for laminae that are not unidirectional. Junctions between laminae with dissimilar carbon fibers serve as thermocouple junctions. The thermocouple sensitivity is high when the dissimilar fibers are intercalated to be n-type and p-type.

By controlling the composite lay-up and/or the curing pressure, an apparently negative resistance can be attained in the through-thickness direction, due to entropy-driven electron backflow.

The glass transition and melting of a thermoplastic polymer matrix upon heating cause matrix molecular movements, which affect the longitudinal electrical resistance of the composite. The resistance is more sensitive to the glass transition than DSC.

The quality of composite-composite joints obtained by adhesion or fastening is revealed by measuring the contact resistance of the joint. For adhesive joints, monitoring the joints during bonding and debonding gives information on the conditions for attaining good

bonding. The quality of composite-concrete joints obtained by adhesion is revealed by measuring the apparent longitudinal resistance of the composite.

REFERENCES

1. W. F. A. Davies, *J. Phys.*, D: App. Phys., **7**, 120–130 (1974).
2. W. J. Gadja, Report RADC-TR-78-158, A059029, 1978.
3. P. Li, W. Strieder, and T. Joy, *J. Comp. Mater.*, **16**, 53–64 (1982).
4. T. Choi, P. Ajmera, and W. Strieder, *J. Comp. Mater.*, **14**, 130–141 (1980).
5. T. Joy and W. Strieder, *J. Comp. Mater.*, **13**, 72–78 (1979).
6. K. W. Tse and C. A. Moyer, *Mater. Sci. and Eng.*, **49**, 41–46 (1981).
7. V. Volpe, *J. Comp. Mater.*, **14**, 189–198 (1980).
8. V. G. Shevchenko, A. T. Ponomarenko, and N. S. Enikolopyan, *Int. J. Appl. Electromagnetics in Materials*, **5**(4), 267–277 (1994).
9. X. B. Chen and D. Billaud, *Ext. Abstr. Program-20th Bienn. Conf. Carbon*, 1991, pp. 274–275.
10. X. Wang and D. D. L. Chung, *Composite Interfaces*, **5**(3), 191–199 (1998).
11. X. Wang and D. D. L. Chung, *Polymer Composites*, **18**(6), 692–700 (1997).
12. X. Wang and D. D. L. Chung, *Carbon*, **35**(5), 706–709 (1997).
13. X. Wang and D. D. L. Chung, *J. Mater. Res.*, **14**(11), 4224–4229 (1999).
14. S. Wang and D. D. L. Chung, *Composite Interfaces*, **6**(6), 497–506 (1999).
15. S. Wang and D. D. L. Chung, *Polymer Composites*, in press.
16. X. Luo and D. D. L. Chung, *Composites Sci. Tech.*, in press.
17. N. Muto, H. Yanagida, T. Nakatsuji, M. Sugita, Y. Ohtsuka, and Y. Arai, *Smart Mater. Struct.*, **1**, 324–329 (1992).
18. X. Wang, X. Fu, and D. D. L. Chung, *J. Mater. Res.*, **14**(3), 790–802 (1999).
19. X. Wang and D. D. L. Chung, *Composites: Part B*, **29B**(1), 63–73 (1998).
20. P. E. Irving and C. Thiogarajan, *Smart Mater. Struct.*, **7**, 456–466 (1998).
21. M. X. Xu, W. G. Liu, Z. X. Gao, L. P. Fang, and K. D. Yao, *J. Appl. Polymer Sci.*, **60**(10), 1595–1599 (1996).
22. X. Wang, S. Wang, and D. D. L. Chung, *J. Mater. Sci.*, **34**(11), 2703–2714 (1999).
23. N. Muto, H. Yanagida, M. Miyayama, T. Nakatsuji, M. Sugita, and Y. Ohtsuka, *J. Ceramic Soc. Japan*, **100**(4), 585–588 (1992).
24. N. Muto, H. Yanagida, T. Nakatsuji, M. Sugita, Y. Ohtsuka, Y. Arai, and C. Saito, *Adv. Composite Mater.*, **4**(4), 297–308 (1995).
25. R. Prabhakaran, *Experimental Techniques*, **14**(1), 16–20 (1990).
26. M. Sugita, H. Yanagida, and N. Muto, *Smart Mater. Struct.*, **4**(1A), A52–A57 (1995).
27. A. S. Kaddour, F. A. R. Al-Salehi, S. T. S. Al-Hassani, and M. J. Hinton, *Composites Sci. Tech.*, **51**, 377–385 (1994).
28. O. Ceysson, M. Salvia, and L. Vincent, *Scripta Materialia*, **34**(8), 1273–1280 (1996).
29. K. Schulte and Ch. Baron, *Composites Sci. Tech.*, **36**, 63–76 (1989).
30. K. Schulte, *J. Physique IV*, Colloque C7, **3**, 1629–1636 (1993).
31. J. C. Abry, S. Bochard, A. Chateauminois, M. Salvia, and G. Giroud, *Composites Sci. Tech.*, **59**(6), 925–935 (1999).
32. A. Tedoroki, H. Kobayashi, and K. Matuura, *JSME Int. J. Series A-Solid Mechanics Strength of Materials*, **38**(4), 524–530 (1995).
33. S. Hayes, D. Brooks, T. Liu, S. Vickers, and G. F. Fernando, *Proc. SPIE-the Int. Soc. for Optical Engineering*, V. 2718 (Smart Structures and Materials 1996: Smart Sensing, Processing, and Instrumentation), SPIE, Bellingham, WA, 1996, pp. 376–384.
34. R. Schueler, S. P. Joshi, and K. Schulte, *Proc. SPIE-The Int. Soc. Optical Engineering*, Vol. 3041, Soc. Photo-Optical Instrumentation Engineers, Bellingham, WA, 1997, pp. 417–426.
35. S. Wang and D. D. L. Chung, *Composites:* Part B, **30**(6), 591–601 (1999).
36. S. Wang and D. D. L. Chung, *Composite Interfaces*, **6**(6), 519–530 (1999).
37. S. Wang and D. D. L. Chung, *Composites:* Part B, **30**(6), 579–590 (1999).
38. J. A. Kuphal, L. H. Sperling, and L. M. Robeson, *J. Appl. Polym. Sci.*, **42**, 1525–1535 (1991).
39. A. L. Simal and A. R. Martin, *J. Appl. Polym. Sci.*, **68**, 453–474 (1998).
40. Ch. R. Davis, *J. Appl. Polym. Sci.*, **62**, 2237–2245 (1996).
41. B. G. Risch and G. L. Wilkes, *Polymer*, **34**, 2330–2343 (1993).
42. H. J. Oswald, E. A. Turi, P. J. Harget, and Y. P. Khanna, *J. Macromol. Sci. Phys.*, **B13**(2), 231–254 (1977).
43. J. U. Otaigbe and W. G. Harland, *J. Appl. Polym. Sci.*, **36**, 165–175 (1988).
44. M. E. Brown, *Introduction to Thermal Analysis: Techniques and Application*, Chapman and Hall, New York (1988), p. 25.
45. C. H. Do, E. M. Pearce, and B. J. Bulkin, *J. Polym. Sci.*, Part A: Polym. Chem., **25**, 2409–2424 (1987).
46. M. C. Gupta and S. G. Viswanath, *J. Thermal Analysis*, **47**(4), 1081–1091 (1996).
47. N. Avramova, *Polym. & Polym. Comp.*, **1**(4), 261–274 (1993).
48. A. L. Simal and A. R. Martin, *J. Appl. Polym. Sci.*, **68**, 441–452 (1998).
49. I. M. Fouda, M. M. El-Tonsy, F. M. Metawe, H. M. Hosny, and K. H. Easawi, *Polym. Testing*, **17**(7), 461–493 (1998).
50. I. M. Fouda, E. A. Seisa, and D. A. El-Farahaty, *Polym. Testing*, **15**(1), 3–12 (1996).
51. L. M. Yarisheva, L. Yu Kabal'nova, A. A. Pedy, and A. L. Volynskii, *J. Therm. Analysis*, **38**(5), 1293–1297 (1992).
52. Z. Mei and D. D. L. Chung, *Polymer Composites*, **21**(5) (2000).
53. H.-Y. Wu, S. Lee, and J.-Y. Wang, *J. Mater. Proc. Tech.*, **75**(1–3), 173–179 (1998).
54. S. Church, J. Day, and B. Wild, *Materials World*, **4**(7), 385–386 (1996).
55. S. P. Godfrey, P. L. Threadgill, and M. Strangewood, *High-Temperature Ordered Intermetallic Alloys VI*, Materials Research Society Symp. Proc. **364**(2), Materials Research Society, Pittsburgh, PA, USA, 1995, p. 793–798.
56. H. R. Hwang and R. Y. Lee, *J. Mater. Sci.*, **31**(9), 2429–2435 (1996).
57. Z. C. Wang, N. Ridley, G. W. Lorimer, K. Knauss, and G. A. D. Briggs, *J. Mater. Sci.*, **31**(19), 5199–5206 (1996).
58. M. F. Vallat, M. Stachnik, and J. Schultz, *J. Adhesion*, **58**(3–4), 183–190 (1996).
59. R. Pitchumani, S. Ranganathan, R. C. Don, J. W. Gillespie, Jr., and M. A. Lamontia, *Int. J. Heat Mass Transfer*. **39**(9), 1883–1897 (1996).
60. A. C. Loos and M. Li, *J. Thermoplastic Composite Materials*, **7**(4), 280–310 (1994).
61. E. J. Jun, T. W. Kim, and W. I. Lee, *High Temperatures-High Pressures*, **22**(6), 655–661 (1990).
62. J. Jou, C. Liu, J. Liu, and J. King, *J. Appl. Polymer Sci.*, **47**(7), 1219–1232 (1993).

63. R. S. Raghava and R. W. Smith, *J. Polymer Sci.*, Part B-Polymer Physics, **27**(12), 2525–2551 (1989).
64. A. G. Mikos, *Polymer*, **30**(1), 84–91 (1989).
65. G. R. Hamed, *Rubber Chem. Tech.*, **61**(3), 548–553 (1988).
66. J. C. Howes and A. C. Loos, *Proc. American Soc. Composites, 2nd Technical Conf.*, Technomic Publ. Co., Lancaster, PA, USA, 1987, p. 110–119.
67. G. R. Hamed and C.-H. Shieh, *J. Polymer Sci.*, Polymer Physics Ed., **21**(8), 1415–1425 (1983).
68. L. Bothe and G. Rehage, *Rubber Chem. Tech.*, **55**(5), 1308–1327 (1982).
69. G. R. Hamed, *Rubber Chem. Tech.*, **54**(3), 576–595 (1981).
70. C. K. Rhee and J. C. Andries, *Rubber Chem. Tech.*, **54**(1), 101–114 (1981).
71. P. G. de Gennes, *J. Chem. Phys.*, **55**(2), 572–579 (1971).
72. Y. H. Kim and R. P. Wool, *Macromolecules*, **16**(7), 1115–1120 (1983).
73. R. P. Wool, *Rubber Chem. Tech.*, **57**(2), 307–319 (1984).
74. Z. Mei and D. D. L. Chung, *Int. J. Adh. Adh.*, **20**, 173–175 (2000).
75. S. Dixon, C. Edwards, and S. B. Palmer, *Ultrasonics*, **32**, 425430 (1994).
76. V. K. Winston, *Int. SAMPE Symp. Exhib.*, (Proc.), **43**, 1428–1437 (1998).
77. Z. Mei and D. D. L. Chung, *Int. J. Adh. Adh.*, **20**, 135-139 (2000).
78. Z. Mei and D. D. L. Chung, *Int. J. Adh. Adh.*, **20**, 273–277 (2000).
79. X. Luo and D. D. L. Chung, *Polym. Eng. Sci.*, **40**, 1505 (2000).
80. H. A. Toutanji, *Composite Structures*, **44**(2), 155–161 (1999).
81. H. A. Toutanji and T. El-Korchi, *J. Composites for Construction*, **3**(1), 38–45 (1999).
82. Y. Lee and S. Matsui, *Tech. Reports Osaka University*, **48** (2319–2337), 247–254 (1998).
83. E. K. Lau, A. S. Mosallam, and P. R. Chakrabarti, *Int. SAMPE Tech. Conf.*, SAMPE, Covina, CA, Vol. 30, 1998, p. 293–302.
84. A. Liman and P. Hamelin, *Proc. Int. Conf. Computer Methods in Composite Materials*, CADCOMP, 1998, Computational Mechanics Publ., Ashurst, England, pp. 569–578.
85. P. Balaguru and S. Kurtz, *Proc. Int. Seminar on Repair and Rehabilitation of Reinforced Concrete Structures: The State of the Art 1998*, ASCE, Reston, VA, pp. 155–168.
86. A. Nanni and W. Gold, *Proc. Int. Seminar on Repair and Rehabilitation of Reinforced Concrete Structures: The State of the Art 1998*, ASCE, Reston, VA, pp.144–154.
87. H. A. Toutanji and T. El-Korchi, *Proc. Int. Seminar on Repair and Rehabilitation of Reinforced Concrete Structures: The State Of the Art 1998*, ASCE, Reston, VA, pp. 134–143.
88. Z. Geng, M. J. Chajes, T. Chou, and D. Y. Pan, *Composites Sci. Tech.*, **58**(8), 1297–1305 (1998).
89. I. Gergely, C. P. Pantelides, R. J. Nuismer, and L. D. Reaveley, *J. Composites for Construction*, **2**(4), 165–174 (1998).
90. H. N. Garden and L. C. Hollaway, *Composites*, Part B, **29**(4), 411–424 (1998).
91. K. Kikukawa, K. Mutoh, H. Ohya, Y. Ohyama, H. Tanaka, and K. Watanabe, *Composite Interfaces*, **5**(5), 469–478 (1998).
92. M. Xie and V. M. Karbhari, *J. Composite Mater.*, **32**(21), 1894–1913 (1998).
93. V. M. Karbhari, M. Engineer, and D. A. Eckel II, *J. Mater. Sci.*, **32**(1), 147–156 (1997).
94. D. P. Henkel and J. D. Wood, *NDT & e International*, **24**(5), 259–264 (1991).
95. A. K. Pandey and M. Diswas, *Journal of Sound & Vibration*, **169**(1), 3–17 (1994).
96. Z. Mei and D. D. L. Chung, *Cem. Concr. Res.*, **30(5)**, 799–802 (2000).